

21 Jan 2024

Dielectric Permittivity Of PZT 95/5 Ferroelectric Ceramics And 0.27PIN-PMN-0.26PT Single Crystals Under Pulsed High Electric Fields

Sergey I. Shkuratov

Jason Baird

Missouri University of Science and Technology, jbaird@mst.edu

Vladimir G. Antipov

Christopher S. Lynch

Follow this and additional works at: https://scholarsmine.mst.edu/min_nuceng_facwork

 Part of the [Explosives Engineering Commons](#)

Recommended Citation

S. I. Shkuratov et al., "Dielectric Permittivity Of PZT 95/5 Ferroelectric Ceramics And 0.27PIN-PMN-0.26PT Single Crystals Under Pulsed High Electric Fields," *Journal of Applied Physics*, vol. 135, no. 3, article no. 034101, American Institute of Physics, Jan 2024.

The definitive version is available at <https://doi.org/10.1063/5.0185734>

This Article - Journal is brought to you for free and open access by Scholars' Mine. It has been accepted for inclusion in Mining Engineering Faculty Research & Creative Works by an authorized administrator of Scholars' Mine. This work is protected by U. S. Copyright Law. Unauthorized use including reproduction for redistribution requires the permission of the copyright holder. For more information, please contact scholarsmine@mst.edu.

RESEARCH ARTICLE | JANUARY 17 2024

Dielectric permittivity of PZT 95/5 ferroelectric ceramics and 0.27PIN-PMN-0.26PT single crystals under pulsed high electric fields


Sergey I. Shkuratov ; Jason Baird ; Vladimir G. Antipov; Christopher S. Lynch 




J. Appl. Phys. 135, 034101 (2024)

<https://doi.org/10.1063/5.0185734>



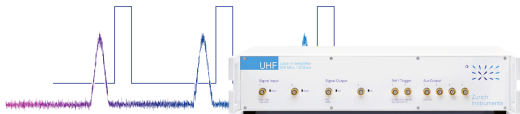


Lock-in Amplifier



Zurich Instruments

Find out more



Boxcar Averager

Boost Your Optics and Photonics Measurements

Dielectric permittivity of PZT 95/5 ferroelectric ceramics and 0.27PIN-PMN-0.26PT single crystals under pulsed high electric fields

Cite as: J. Appl. Phys. 135, 034101 (2024); doi: 10.1063/5.0185734

Submitted: 1 November 2023 · Accepted: 23 December 2023 ·

Published Online: 17 January 2024



Sergey I. Shkuratov,^{1,a)} Jason Baird,^{1,2} Vladimir G. Antipov,¹ and Christopher S. Lynch³

AFFILIATIONS

¹Loki Incorporated, Norwood, Missouri 65717, USA

²Department of Mining and Nuclear Engineering, Missouri University of Science and Technology, Rolla, Missouri 65409-0450, USA

³Bourns College of Engineering, University of California at Riverside, California 92521, USA

^{a)}Author to whom correspondence should be addressed: shkuratov@lokiconsult.com

ABSTRACT

The dependence of the dielectric permittivity of ferroelectric materials on electric field magnitude impacts the performance of ferroelectric devices. In a ferroelectric generator, a shock wave travels through the ferroelectric element and depolarizes it, and surface charges are released from the element electrodes, resulting in the generation of a megawatt power level for several microseconds. The dielectric properties of the compressed and uncompressed zones of the ferroelectric element affect the generated voltage and energy. The results of previous studies indicate that the low-field dielectric permittivity of poled $\text{Pb}_{0.99}(\text{Zr}_{0.95}\text{Ti}_{0.05})_{0.98}\text{Nb}_{0.02}\text{O}_3$ (PZT 95/5) ferroelectrics in the uncompressed zone differs significantly from the high-field permittivity. Herein, the results are presented from the experimental investigation of the high-field permittivity of poled uncompressed PZT 95/5 ferroelectric ceramics and films, PZT 52/48 ferroelectric ceramics, and rhombohedral $0.27\text{Pb}(\text{In}_{1/2}\text{Nb}_{1/2})\text{O}_3-0.47\text{Pb}(\text{Mg}_{1/3}\text{Nb}_{2/3})\text{O}_3-0.26\text{PbTiO}_3$ (0.27PIN-PMN-0.26PT) and $0.68\text{Pb}(\text{Mg}_{1/3}\text{Nb}_{2/3})\text{O}_3-0.32\text{PbTiO}_3$ (0.68PMN-0.32PT) ferroelectric single crystals. The dependences of the permittivity on the electric field were determined using a pulsed electric field ranging from 0.1 to 10 kV/mm. The data indicate that the application of a pulsed high electric field results in a fourfold increase in the relative permittivity of PZT 95/5 ceramics and films over the small signal value (from 300 to 1200), and a threefold increase in the permittivity of single-domain $[111]_c$ cut and poled 0.27PIN-PMN-0.26PT crystals (from 700 to 2100), while a high electric field does not have a significant impact on the permittivity of PZT 52/48 ceramics or 0.27PIN-PMN-0.26PT and 0.68PMN-0.32PT crystals cut and poled in the domain engineered $[001]_c$ or $[011]_c$ direction.

© 2024 Author(s). All article content, except where otherwise noted, is licensed under a Creative Commons Attribution (CC BY) license (<https://creativecommons.org/licenses/by/4.0/>). <https://doi.org/10.1063/5.0185734>

I. INTRODUCTION

Electrical energy can be generated in ferroelectric materials through stress-induced dipole reorientation or a phase transformation to a non-polar phase. Compact autonomous power generation devices, i.e., shock wave driven ferroelectric generators (FEGs), that exploit the spontaneous polarization of ferroelectric materials are capable of producing hundreds of kilovolts of electric potential, kiloamperes of electrical current, and megawatt power levels for brief intervals of time.^{1–9} Several types of ferroelectric ceramics and single crystals can be depolarized under shock compression and,

thus, can be used in high-power FEGs.^{1–3,6–15} Most FEGs are designed to operate with the shock wave oriented to travel parallel to the electrodes as shown in Fig. 1.

As the shock wave passes through the ferroelectric element, its volume is divided into two zones. The compressed zone is the portion through which the shock wave has already passed. For the case where the shock wave travels parallel to the electrodes, the ferroelectric element behaves as two nonlinear capacitors in parallel as shown in Fig. 1. The ferroelectric material in the compressed zone is depolarized and generally has a lower dielectric permittivity than

26 March 2024 21:11:50

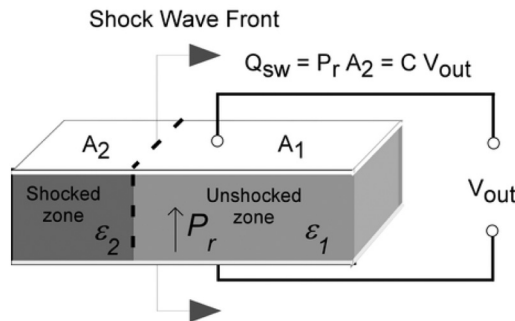


FIG. 1. Equivalent circuit for the shock depolarization process where the shock has propagated part way across the specimen. Q_{sw} is the stress-induced charge. P_r is the remanent polarization vector. V_{out} is the generated voltage. A_1 and A_2 are the areas of electrodes of uncompressed and compressed zones of the ferroelectric element, respectively. ϵ_1 and ϵ_2 are the permittivity of uncompressed and compressed zones, respectively. C is the capacitance of the element.

the uncompressed material. At zero electric field, a poled ferroelectric has a surface charge density equivalent to the remanent polarization of the material. This is referred to as the screening charge that terminates the normal component of the electric displacement. Compression reduces or eliminates the polarization either through a ferroelastic effect or a phase transformation. This results in the screening charge becoming free charge on the electrodes of a capacitor. In the equivalent circuit of Fig. 1, the compressed zone and uncompressed zone share the same electrodes and are, thus, represented as two capacitors in parallel. When the polarization is reduced by compressive stress in the shocked zone, the screening charge is redistributed across the two capacitors. Under open circuit conditions, a high voltage is generated.

The time dependent voltage generated is a function of the polarizability of the two zones. If the induced polarization is close enough to linear that it can be approximated as a linear dielectric, the capacitance of the ferroelectric element can be determined from the geometric dimensions of the element, the dielectric properties of the ferroelectric material in the uncompressed and compressed zones under high electric fields, the volume of material in each of these zones, and the orientation of the shock relative to the electrodes (parallel or perpendicular).

This approach can introduce significant error because the polarizability of the material is nonlinear and, in some cases, hysteretic. Rather than using the small-field permittivity obtained from the slope of the electric displacement vs electric field curve at zero electric field, the high-field permittivity is obtained from the ratio of the peak electric field to the peak electric displacement change. There are large differences between the low-field and the high-field permittivity. The high-field induced polarization of the material in the uncompressed zone is important in the design of pulsed power devices because it has a significant impact on their performance. The induced polarization is a function of intrinsic piezoelectric effect, i.e., the component associated with distortions of the perovskite crystal structure, and extrinsic effects (the component associated

with domain wall motion). Intrinsic polarization changes tend to display little hysteresis, whereas extrinsic polarization changes tend to be hysteretic. The high-field polarizability of ferroelectric materials loaded in the microsecond time scale has not been well characterized.

Past work has focused on understanding the material response based on shock loading. The dielectric permittivity of shock-compressed lead zirconate titanate composition $\text{PbZr}_{0.95}\text{Ti}_{0.05}\text{O}_3$ doped with 2% of Nb (PZT 95/5) during shock transit under high electric fields has been investigated by Lysne,^{1,16–18} Setchell *et al.*,¹⁹ and Wu *et al.*²⁰ The results of these studies^{1,16–23} indicate that high electric fields have a significant impact on the permittivity of poled PZT 95/5 in the uncompressed zone, while the permittivity of the depolarized material in the compressed zone has little correlation with electric field. Some quasi-static high pressure measurements of permittivity have been reported. The dielectric properties of PZT 95/5 under hydrostatic stress and high static electric field were investigated by Valadez *et al.*²¹ Their experimental results indicate that at zero stress under an electric field of 1 kV/mm, the permittivity of poled PZT 95/5, $\epsilon(1 \text{ kV/mm}) = 1119$, was greater by a factor of 3.7 than the low-field permittivity.

Shock wave ferroelectric generators produce electric fields exceeding 7 kV/mm across their ferroelectric elements.^{1–5,9,24} Before the shock has completely propagated across the ferroelectric element, a part of the element is in the polarized uncompressed state. Therefore, understanding electrical power output during shock transit requires a better understanding of the high electric field dielectric permittivity of the poled ferroelectric material in the uncompressed zone.

Measurement of the dielectric properties of ferroelectrics using shock wave loading experiments is a challenging task because of the complex electrical response of the uncompressed and compressed zones of the ferroelectric element and the difficulty of isolating the response of the material in the compressed zone from the response of the material in the uncompressed zone from the single output signal. This led to the development reported here of an experimental arrangement suitable for measuring the polarization response to a high electric field applied in the microsecond time frame.

II. EXPERIMENTAL

To measure the permittivity of poled uncompressed ferroelectric materials under pulsed high electric fields, an experimental system was developed that provided the magnitude and dynamics of charging current and voltage under testing conditions that are very close to those that occur in the uncompressed zone of an FEG. The rise time of the voltage generated by an FEG lies in the microsecond range.^{1–5,9,24} The experimental system (Fig. 2) was based on a Tesla pulser. A DC high voltage power supply charged the primary capacitor bank of the Tesla pulser. When the charging voltage reached the desired level, the spark gap switch closed, the capacitor bank discharged into the Tesla primary winding, and a high voltage pulse was applied to the ferroelectric element under test. The voltage across the ferroelectric element was monitored with a Tektronix P6015A high voltage probe or North Star PVM-5 probe. The current was monitored with Pearson 411 and 4100 current probes.

26 March 2024 21:11:50

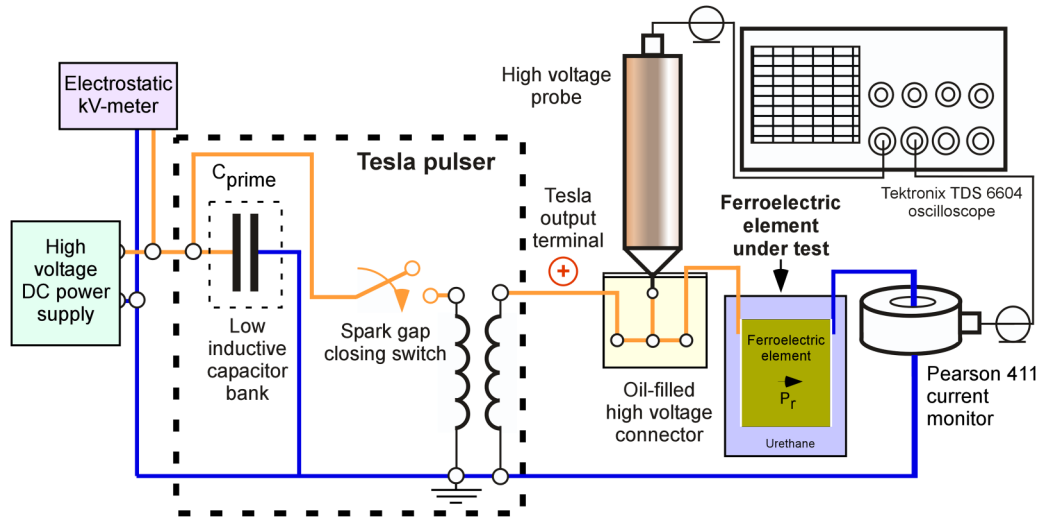


FIG. 2. Schematic of the experimental system used to investigate the dielectric permittivity of ferroelectric materials under pulsed high electric fields under ambient conditions.

In all experiments, the polarity of the voltage generated across the ferroelectric elements under test was identical to the voltage polarity for FEGs operating in the high voltage mode; i.e., the applied pulsed electric field was oriented to increase the polarization of the ferroelectric elements. This would correspond to the second pulse used in PUND testing where the first voltage loading is used to induce ferroelectric polarization reorientation, resulting in remanent polarization, and the second pulse is used to measure the change of polarization of the material once in the poled state plus any additional charge needed to charge the associated circuit.²⁵

$\text{PbZr}_{0.95}\text{Ti}_{0.05}\text{O}_3$ doped with 2% of Nb (PZT 95/5), $\text{PbZr}_{0.52}\text{Ti}_{0.48}\text{O}_3$ doped with 1% of Nb (PZT 52/48) ferroelectric ceramics, rhombohedral $0.27\text{Pb}(\text{In}_{1/2}\text{Nb}_{1/2})\text{O}_3-0.47\text{Pb}(\text{Mg}_{1/3}\text{Nb}_{2/3})\text{O}_3-0.26\text{PbTiO}_3$ (0.27PIN-PMN-0.26PT) single crystals, and rhombohedral $0.68\text{Pb}(\text{Mg}_{1/3}\text{Nb}_{2/3})\text{O}_3-0.32\text{PbTiO}_3$ (0.68PMN-0.32PT) crystals were investigated. These ferroelectric materials are used in high-power applications.^{1-5,9,10,12,13} TRS Technologies Inc. provided the PZT 95/5 ceramic and film elements, 0.27PIN-PMN-0.26PT crystals, and 0.68PMN-0.32PT crystals. The 0.27PIN-PMN-0.26PT crystal elements were cut and poled in the $[001]_c$, $[011]_c$, or $[111]_c$ directions. The 0.68PMN-0.32PT crystal elements were cut and poled in the $[001]_c$ or $[011]_c$ directions. EDO Ceramic Corp. provided the PZT 52/48 ceramic elements (trade name: EC-64).

III. PERMITTIVITY OF FERROELECTRIC MATERIALS UNDER PULSED HIGH ELECTRIC FIELDS

A. PZT 95/5 ceramics

Pulsed electric field permittivity measurements were performed on PZT 95/5 ceramic elements with electrode areas of $12.7 \times 12.7 \text{ mm}^2$ and two different thicknesses, 5 and 1 mm, and

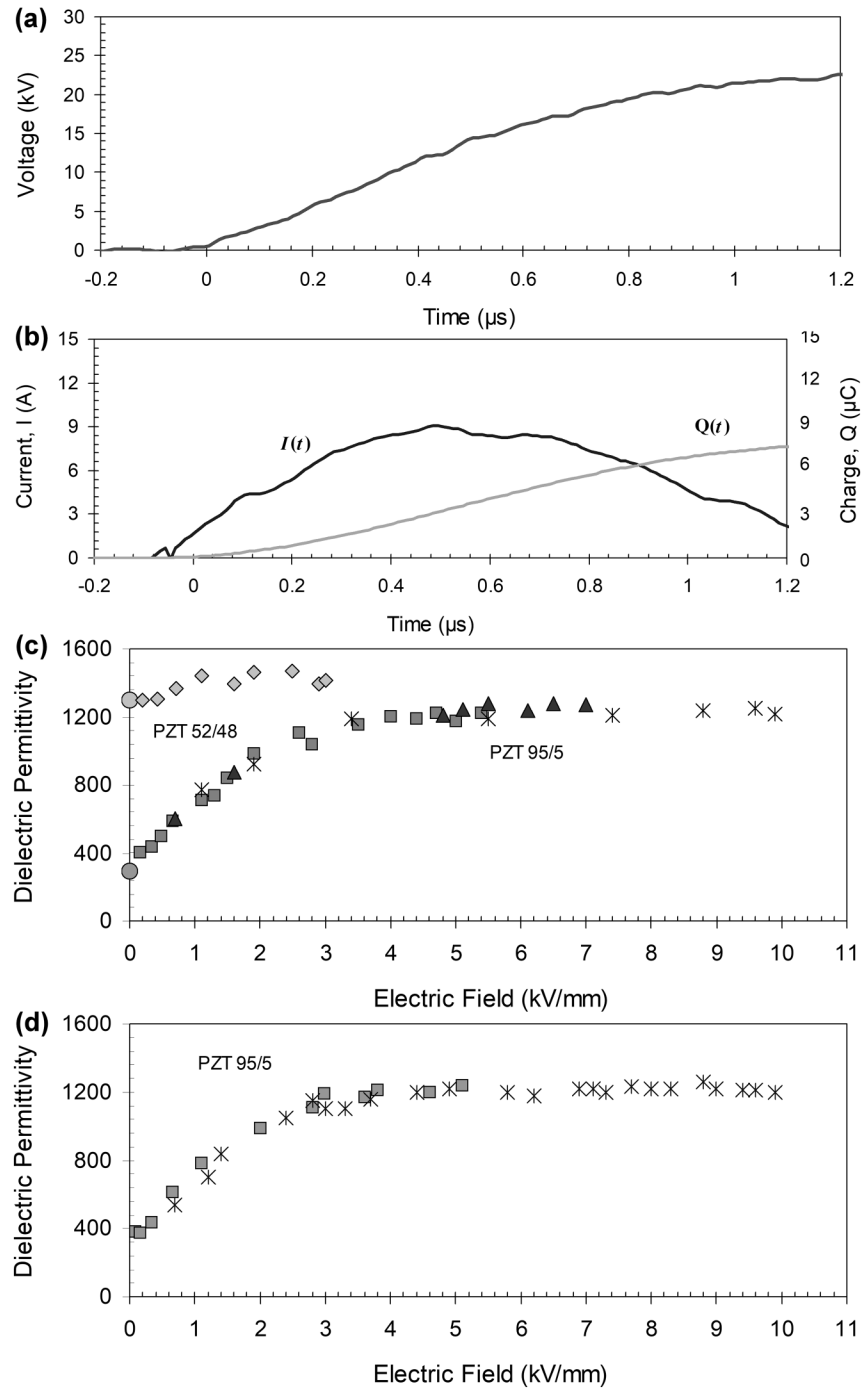
PZT 95/5 films with a thickness of $32 \mu\text{m}$ and an electrode area of $4.0 \times 6.3 \text{ mm}^2$. The remanent polarization of the elements was $P_r = 34 \mu\text{C}/\text{cm}^2$. The elements were encapsulated with a urethane compound as an electrical insulating material similar to that used in our FEGs. The results of experimental investigations of electric breakdown in ferroelectrics under ambient conditions^{26,27} indicate that near the breakdown point, the electric field causes the formation of conductive channels. It was experimentally demonstrated^{26,27} that the formation of tubular channels extending from an initial conducting crack occurred in the direction of the applied electric field. To avoid irreversible changes in ferroelectric materials and a corresponding leakage current, we performed the permittivity measurements at electric fields 30% lower than the breakdown field of the investigated ferroelectric elements.

The PZT 95/5 composition is just to the ferroelectric side of the antiferroelectric-ferroelectric (AFE-FE) phase boundary.²⁸ Upon cooling from high temperature, the material at room temperature is in the ferroelectric phase. Application of a strong electric field drives the material into a higher volume poled ferroelectric phase; i.e., the material remains in the ferroelectric phase under a strong electric field.

Figure 3(a) shows the voltage waveform generated across a poled PZT 95/5 element of $5 \times 12.7 \times 12.7 \text{ mm}^3$. The rise time of the voltage pulse was $1.2 \mu\text{s}$, and the amplitude was 22.5 kV (the electric field was $4.5 \text{ kV}/\text{mm}$). Figure 3(b) shows the waveforms of the charging current and electric charge transferred into the element determined from a time integral of the charging current.

The capacitance of the PZT 95/5 [Figs. 3(a) and 3(b)] obtained from a low-field measurement performed before the high-field experiment was 88 pF, and the corresponding relative dielectric permittivity was $\epsilon = 307$. The instantaneous capacitance of the ferroelectric element under pulsed electric fields, $C(t)$, was

26 March 2024 21:11:50



26 March 2024 21:11:50

FIG. 3. (a) Waveform of the voltage generated across a PZT 95/5 element of $5 \times 12.7 \times 12.7 \text{ mm}^3$. (b) Waveforms of the charging current and electric charge transferred into the element. (c) Experimentally obtained dependences of the permittivity of PZT 95/5 ceramic elements of $5 \times 12.7 \times 12.7 \text{ mm}^3$ (squares), PZT 95/5 ceramic elements of $1 \times 12.7 \times 12.7 \text{ mm}^3$ (triangles), and PZT 95/5 films of $32 \mu\text{m} \times 4.0 \text{ mm} \times 6.3 \text{ mm}$ (asterisks) on a pulsed electric field at the first application of the electric field. The permittivity of PZT 52/48 elements of $5 \times 12.7 \times 12.7 \text{ mm}^3$ is shown by the diamonds. The low-field permittivity for both ferroelectrics is represented by the circles. (d) Experimentally obtained permittivity of two PZT 95/5 ceramic elements: $5 \times 12.7 \times 12.7 \text{ mm}^3$ (squares) and two PZT 95/5 film elements of $32 \mu\text{m} \times 4.0 \text{ mm} \times 6.3 \text{ mm}$ (asterisks) exposed to a high voltage multiple times.

determined from

$$C(t) = \frac{Q(t)}{V(t)}, \quad (1)$$

where $V(t)$ is the voltage generated across the ferroelectric element and $Q(t)$ is the charge transferred into the element at time t .

The relative dielectric permittivity of the ferroelectric material is

$$\epsilon(t) = \frac{Q(t) d}{\epsilon_0 V(t) A}, \quad (2)$$

where A is the area of the ferroelectric element electrodes, d is the thickness of the ferroelectric element, and ϵ_0 is the dielectric permittivity of free space.

Substituting parameters from the experiment in Figs. 3(a) and 3(b) [$V(1.2 \mu\text{s}) = 22.5 \text{ kV}$, $d = 5 \text{ mm}$, $A = 1.61 \text{ cm}^2$, and $Q(1.2 \mu\text{s}) = 7.6 \mu\text{C}$] into Eq. (2) gives the relative permittivity of PZT 95/5 under an electric field of 4.5 kV/mm , $\epsilon(4.5 \text{ kV/mm}) = 1182$, which is significantly higher than the low-field permittivity.

Figure 3(c) shows the experimentally obtained dependence of the permittivity of sixteen 5 mm thick PZT 95/5 ceramic elements, eight 1 mm thick PZT 95/5 ceramic elements, and eight $32 \mu\text{m}$ thick PZT 95/5 film elements as a function of pulsed electric field. In these experiments, each PZT 95/5 element was under a high voltage test only once. This was to provide experimental conditions that were identical to those in shock wave driven FEGs, where the elements are exposed to a high electric field only once.

The experimental results [Fig. 3(c)] indicate that the high-field permittivity of PZT 95/5 films is very close to those obtained for PZT 95/5 ceramic elements with 1 mm and 5 mm thickness (the asterisks, triangles, and squares in Fig. 3). The element thickness and the area of the element electrodes did not have a significant impact on the permittivity of PZT 95/5 under a pulsed electric field.

Ceramic PZT compositions have a grain size in the $5\text{--}10 \mu\text{m}$ range. Each grain contains multiple domains. The specimens tested each had a thickness that is many grains thick; thus, the resulting measurements give the volume average response of the materials without displaying thickness effects that would be present in elements with thickness on the order of the grain size.

The experimental data indicate that an increase in the electric field from 0 to 4 kV/mm results in an increase in the permittivity of PZT 95/5 by a factor of 4 ($300\text{--}1200$), while a further increase in the electric field does not result in a significant change in the permittivity.

We measured the capacitance of PZT 95/5 elements with a QuadTech 7600 LCR-meter before and after high voltage experiments. The results of these measurements indicate that the low-field capacitance and the corresponding permittivity practically did not change after the application of a high voltage; i.e., after the high voltage pulse, the low-field permittivity of PZT 95/5 returned to its original value.

In the second experimental series, two PZT 95/5 elements of $5 \times 12.7 \times 12.7 \text{ mm}^3$ and two PZT 95/5 film elements with a thickness of $32 \mu\text{m}$ and an electrode area of $4.0 \times 6.3 \text{ mm}^2$ were exposed

to a high voltage several times. The applied electric field ranged from 0.1 to 10 kV/mm . Figure 3(d) shows the permittivity dependence on the electric field. The obtained results indicate that the application of pulsed high electric fields multiple times results in permittivity levels similar to those observed on the first application.

We conducted experiments with 5 mm thick PZT 95/5 elements at two different voltage rise times, 1.2 and $0.6 \mu\text{s}$. We did not observe a significant impact of the loading rate on the high-field permittivity in the range tested.

B. PZT 52/48 ferroelectric ceramics

PZT 52/48 ferroelectric ceramics are utilized in both shock wave FEGs and non-explosive high-power piezoelectric generators.^{4,5,9,15} We investigated the high electric field permittivity of PZT 52/48 elements with a thickness of 5 mm and an electrode area of $12.7 \times 12.7 \text{ mm}^2$. The remanent polarization of the elements was $P_r = 32 \mu\text{C/cm}^2$.

Figure 4 shows the voltage waveform generated across the poled PZT 52/48 element and the waveforms of the charging current and electric charge transferred into the element. The rise time of the voltage pulse was $1.4 \mu\text{s}$, and the amplitude was 14.4 kV (the electric field was 2.9 kV/mm).

The capacitance of the PZT 52/48 element (Fig. 4) obtained from low-field measurements was 370 pF , and the corresponding low-field dielectric permittivity was $\epsilon = 1293$. Substituting parameters from the experiment in Fig. 4 [$V(1.64 \mu\text{s}) = 14.4 \text{ kV}$, $d = 5 \text{ mm}$, $A = 1.61 \text{ cm}^2$, and $Q(1.64 \mu\text{s}) = 5.8 \mu\text{C}$] into Eq. (2) gives the relative permittivity of poled PZT 52/48 under an electric field of 2.9 kV/mm , $\epsilon(2.9 \text{ kV/mm}) = 1398$, which is close to the low-field permittivity.

The experimentally obtained dependence of the permittivity of PZT 52/48 on a pulsed electric field is marked as diamonds in Fig. 3(c). The experimental results indicate that a pulsed electric field ranging from 0.2 to 3 kV/mm does not have a significant impact on the permittivity of PZT 52/48.

The PZT 52/48 is a composition at the rhombohedral/tetragonal morphotropic phase boundary (MPB).²⁸ This is a region where the eight rhombohedral and six tetragonal variants can coexist. There is a maximum in permittivity as a function of composition at the 52/48 composition because it is easy for domain walls to move in this composition. At a high field, depending on the orientation of particular grains and the local intergranular stress, the field can drive the phase transformations of small regions from the rhombohedral (R) to the tetragonal (T) phase or from T to R , further increasing the polarizability. Domain wall motion in the poled ferroelectric under a strong electric field is countered by intergranular stress buildup because the shapes of the single-domain grains are not compatible. The experimental results indicate that these processes are nearly independent of the loading rate and field amplitudes in the ranges tested.

C. PIN-PMN-PT and PMN-PT single crystals

Relaxor ferroelectric-based PIN-PMN-PT and PMN-PT single crystals are promising materials for high-power applications.^{5,12–15} We investigated rhombohedral 0.27PIN-PMN-0.26PT crystals cut and poled along the $[111]_c$, $[011]_c$, or $[001]_c$ crystallographic

26 March 2024 21:11:50

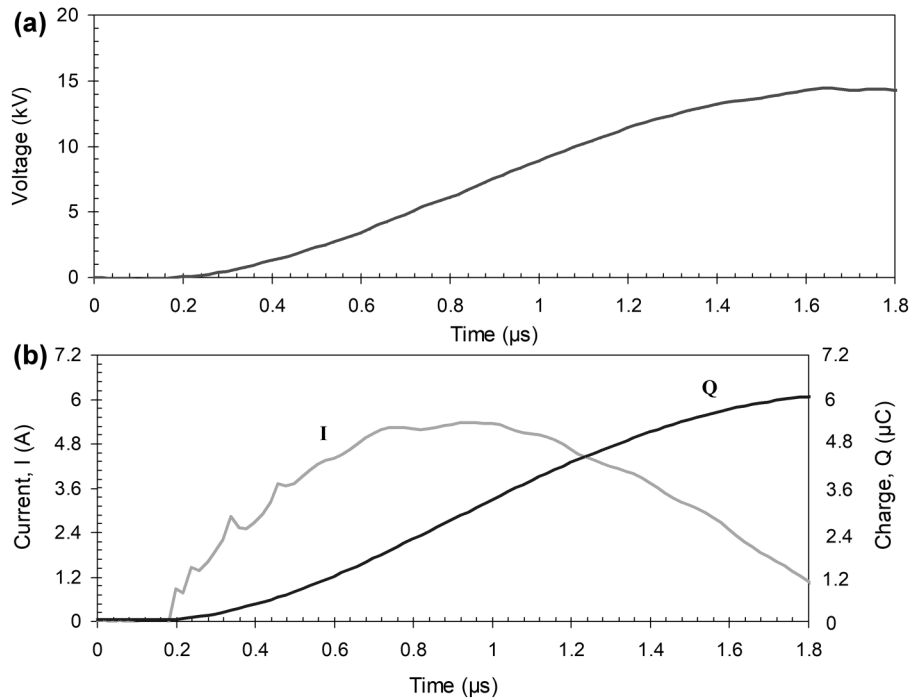


FIG. 4. (a) Waveform of the voltage generated across a PZT 52/48 element of $5 \times 12.7 \times 12.7 \text{ mm}^3$. (b) Waveforms of the charging current and electric charge transferred into the element.

directions. Figures 5(a) and 5(b) show the voltage waveform generated across a single-domain $[111]_c$ cut and poled 0.27PIN-PMN-0.26PT crystal and waveforms of the charging current and electric charge transferred into the element. The rise time of the voltage was $1.2 \mu\text{s}$, and the amplitude was 4.26 kV (the electric field was 4.26 kV/mm). The crystal thickness was 1 mm , and its electrode area $5 \times 5 \text{ mm}^2$. The remanent polarization of the crystals was $P_r = 48 \mu\text{C/cm}^2$.

The low-field capacitance of this 0.27PIN-PMN-0.26PT crystal [Figs. 5(a) and 5(b)] was 160 pF , and the corresponding low-field dielectric permittivity was $\epsilon = 723$. Substituting parameters from the experiment in Figs. 5(a) and 5(b) [$V(-0.85 \mu\text{s}) = 4.26 \text{ kV}$, $d = 1 \text{ mm}$, $A = 0.25 \text{ cm}^2$, and $Q(-0.85 \mu\text{s}) = 1.89 \mu\text{C}$] into Eq. (2) gives $\epsilon(4.26 \text{ kV/mm}) = 2004$ as the relative permittivity of 0.27PIN-PMN-0.26PT crystal under an electric field of 4.26 kV/mm . This is significantly higher than the low-field permittivity.

Figure 5(c) shows the experimentally obtained permittivity of seventeen single-domain 0.27PIN-PMN-0.26PT $[111]_c$ crystals under a pulsed electric field ranging from 0.5 to 7 kV/mm . The permittivity increases from 720 to 2100 with an increase in the applied field from 0 to 3 kV/mm , while a further increase in the electric field does not result in a significant change in the permittivity. We observed similar behavior for the permittivity of PZT 95/5 (Fig. 3).

We also conducted experiments for the secondary application of a high electric field to single-domain 0.27PIN-PMN-0.26PT crystals. Two crystals were exposed to a pulsed high voltage several times. The obtained data [the asterisks in Fig. 5(c)] indicate that the application of a high electric field a few times results in practically the same permittivity levels as it was observed at the first application.

The low-field capacitance and the corresponding permittivity of single-domain 0.27PIN-PMN-0.26PT crystals measured before high voltage experiments were practically equal to those measured after experiments.

Our experimental results indicate that pulsed electric fields ranging from 0.2 to 2 kV/mm do not have a significant impact on the permittivity of rhombohedral multi-domain 0.27PIN-PMN-0.26PT crystals cut and poled in the $[001]_c$ direction (the low-field permittivity 5100 , $P_r = 25 \mu\text{C/cm}^2$) and in the $[011]_c$ direction (the low-field permittivity 3800 , $P_r = 38 \mu\text{C/cm}^2$). We obtained similar results with rhombohedral 0.68PMN-0.32PT crystals cut and poled along the $[001]_c$ or $[011]_c$ direction.

Single crystals do not have grains, but they do contain many domains. In the domain engineered cuts $[001]_c$ and $[011]_c$, there is no driving force for domain wall motion and the domain configuration is stable. This gives rise to very low loss (low hysteresis) and linear dielectric behavior associated with polarization rotation under an applied field. At electric field levels above a transformation field, the $[001]_c$ crystals will undergo a phase transformation from rhombohedral to tetragonal and the $[011]_c$ crystals will undergo a phase transformation from rhombohedral to orthorhombic.²⁹ The effects of phase transformations were not observed in these experiments.

IV. DISCUSSION

An increase in the permittivity of ferroelectrics under a high electric field has an impact on the characteristics of low-power ferroelectric devices and high-power ferroelectric systems operating at high electric field levels. There are several possible reasons for these

26 March 2024 21:11:50

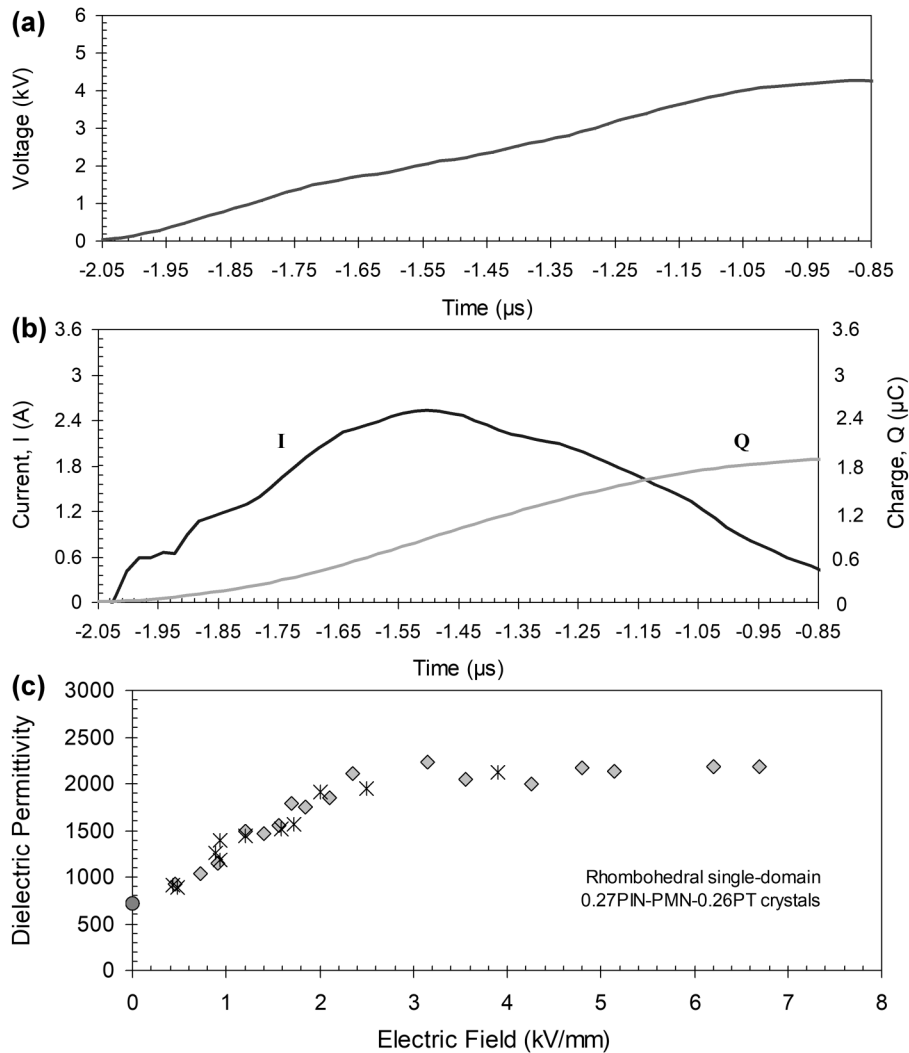


FIG. 5. (a) Waveform of the voltage generated across a rhombohedral single-domain 0.27PIN-PMN-0.26PT crystal of $1 \times 5 \times 5 \text{ mm}^3$ cut and poled along the $[111]_c$ direction. (b) Waveforms of the charging current and electric charge transferred into the crystal. (c) The experimentally obtained dependence of the permittivity of rhombohedral single-domain 0.27PIN-PMN-0.26PT crystals cut and poled in the $[111]_c$ direction on the pulsed electric field for the first application (diamonds). The permittivities of crystals exposed to a high voltage several times are shown by the asterisks. The low-field permittivity is represented by the circle.

26 March 2024 21:11:50

permittivity changes. High polarizability of the ferroelectric material can be one of the reasons a high voltage pulse causes a different permittivity of a poled ferroelectric than is indicated by low-field measurements.

Our experiments do not isolate the different contributions to polarizability. They give the volume average polarization change. Possible sources of the polarization change include intrinsic piezoelectricity (distortion of the crystal structure), domain wall motion (this contributes to hysteresis and heat generation), and phase transformations. PZT 95/5 in the polarized state is in the rhombohedral phase and the electric field is in the direction that further stabilizes the rhombohedral phase; thus, it is unlikely that phase transformation effects are present.

PZT 52/48 is at the MPB, so some amount of shifting between rhombohedral, monoclinic, and tetragonal is likely contributing to the increased polarization under a high electric field applied in the polarization direction. Domain wall motion is known to take place

in the ferroelectric ceramic compositions (PZT 95/5 and PZT 52/48). This contributes to the high-field permittivity.

Domain walls are stable in the domain engineered single crystal cuts $[001]_c$ and $[011]_c$, resulting in permittivity that is independent of the electric field over the range measured. Domain wall motion does take place in the $[111]_c$ single crystals, resulting in an extrinsic contribution to the high-field permittivity.

Polarization change associated with domain wall motion, i.e., extrinsic polarization change, is well known to be time dependent. This is the reason it is important to have data from measurements run at the same time scale as the loading in FEGs.

Defect structures in PZT affect domain wall motion and other material properties.³⁰ Nb is a donor dopant. As discussed in Ref. 31, the donor doping of PZT with Nb increases the resistivity and the mobility of domain walls, while decreasing oxygen vacancy concentration, thus increasing the piezoelectric response. Although the defect structure contributes to the polarizability, bulk

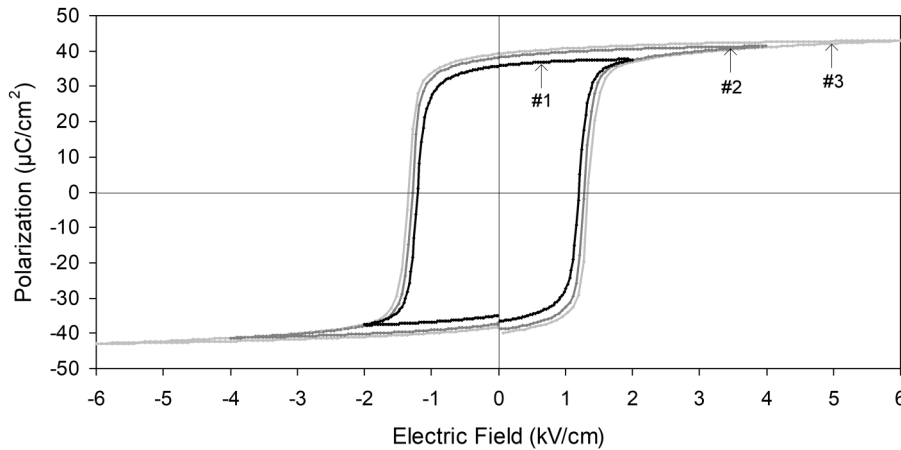


FIG. 6. PZT 95/5 hysteresis loops at different electric fields (AC electric field at 1 Hz): Plot #1—2.0 kV/mm, Plot #2—4.0 kV/mm, and Plot #3—6.0 kV/mm (raw data were provided by TRS Technologies).

measurements like those reported here cannot isolate the effects of defects from other contributions to the polarizability of the material.

In the measurements, the ferroelectric began in a polarized state and the voltage pulse was applied in the direction of the polarization. This is the equivalent of the second positive pulse of a PUND measurement²⁵ following the first positive pulse. Although leakage would result in the measured charge flow, D–E loops are run in the seconds time scale without discernable leakage and these experiments were run in the microseconds time scale. This would further reduce any leakage current effects by multiple orders of magnitude and, thus, leakage effects on the results are not believed to be present.

Figure 6 shows the hysteresis loops at three electric field levels for the 1 mm thick PZT 95/5 ceramic element investigated in this paper. The figure demonstrates how polarizability changes with increasing imposed external electric fields. Logarithmic aging is a well-known phenomenon in PZT where the remanent polarization decreases over time and is another possible reason for permittivity changes. Minor hysteresis loops also occur. When a small cyclic electric field is applied, it will produce a minor hysteresis loop that can be modeled as an ellipse. The area within the ellipse is the dielectric loss per cycle, and the slope is the permittivity; this slope is smaller than the slope found when unloading from a large electric field. There is also a saturation phenomenon at higher electric field where the hysteresis loop flattens out. This flattening of minor hysteresis loops to levels beyond the small-field response (ellipse idealization) is referred to as Rayleigh behavior. The remanent polarization of PZT 95/5 (Fig. 6) is 37.6, 41.3, and 43.0 $\mu\text{C}/\text{cm}^2$ under electric fields of 2.0, 4.0, and 6.0 kV/mm, respectively; i.e., the polarization is directly proportional to the applied electric field.

The high polarizability of PZT 95/5 (Fig. 6) contributes to the increase in its permittivity under a high electric field. Note that a rising electric field might increase the polarization of an uncompressed PZT 95/5 element to a level significantly higher than the initial polarization, resulting in an increase in the stress-induced charge produced by the element during shock transit. It is a complex and dynamic process; nevertheless, the results obtained in this study can be used for the analysis of the operation of ferroelectric systems.

The experimental results obtained in this study for high-field permittivity of PZT 95/5 (Fig. 3) are in agreement with the permittivity of poled PZT 95/5 in the uncompressed zone of the ferroelectric elements during shock wave transit obtained by Setchell *et al.*¹⁹ at 3.4 kV/mm and Wu *et al.*²⁰ at 1.3 kV/mm. For some applications, the ferroelectric element of the FEG is connected to the external circuit through an open switch that is closed when the FEG output voltage reaches the level required for the operation of the external circuit. Until the moment when the switch is closed, the ferroelectric element is operating in the open circuit mode. As a shock wave travels through the element, the volume fraction of the ferroelectric material behind the moving shock front is compressed and depolarized and the volume fraction of material ahead of the shock front has not yet been compressed. The experimental observations are that when the shock is traveling parallel to the electrodes in a transverse FEG, the output voltage reaches the operating level when a portion of ferroelectric materials (from 10% to 50%) is depolarized but the remaining material is in the uncompressed polarized state.^{1–5,9,24,27} The compressed material behaves as a capacitor, with the compressed material dielectric permittivity and a surface charge equal to the shock-induced reduction of remanent polarization. This capacitor is in parallel with a second capacitor (the uncompressed material) that behaves with the uncompressed material dielectric permittivity (Fig. 1).

The voltage produced by a shock-compressed ferroelectric element in the open circuit mode is directly proportional to the amount of stress-released electric charge and inversely proportional to the capacitance of the element,

$$V_{FEG}(t) = \frac{Q_{sw}(t)}{C_{FEG}(t)}, \quad (3)$$

where $V_{FEG}(t)$ is the voltage generated by the ferroelectric element at time t , $Q_{sw}(t)$ is the electric charge released by the element, which is bounded by the initial polarization and the electrode area, and $C_{FEG}(t)$ is the capacitance of the element.

According to Eq. (3), the voltage generated by a partially depolarized PZT 95/5 element of a transverse FEG could be significantly lower than that calculated with the low-field permittivity due

26 March 2024 21:11:50

to the significantly larger high-field permittivity of the uncompressed region of the PZT 95/5 element resulting in a larger capacitance. An increase in the permittivity of uncompressed PZT 95/5 under high electric fields might also have an impact on the ferroelectric element energy density.

Consider a transversely shocked PZT 95/5 ferroelectric element of 24 (thickness) \times 16 (length) \times 25 (width) mm³ with an initial capacitance of 45 pF (typical size for miniature high voltage FEGs^{4,5,9,24,27}). The shock wave propagation direction is parallel to the length of the element (16 mm) and perpendicular to the element polarization (the transverse compression mode). The velocity of the shock wave front is 3.8 mm/ μ s.^{1,2,9} At time $t = 0.7 \mu$ s from the moment when the shock front entered the element, the shock wave has propagated through the element for 2.7 mm (11% of the electrode area and element volume). Assuming complete depolarization of the shocked part of the PZT 95/5 element with $P_r = 34 \mu\text{C}/\text{cm}^2$, the stress-released electric charge is $Q_{sw}(0.7 \mu\text{s}) = 22.6 \mu\text{C}$. This charge remains on the electrodes of the ferroelectric element, resulting in the generation of a high voltage across the element.

During shock wave transit, the capacitance of a transversely shocked element is formed by the capacitance of the compressed part and the capacitance of the uncompressed part in parallel connectivity,

$$C_{FEG}(t) = C_1(t) + C_2(t) = \epsilon_0 \left(\frac{\epsilon_1 A_1}{d} + \frac{\epsilon_2 A_2}{d} \right), \quad (4)$$

where $C_1(t)$ and $C_2(t)$ are the capacitances of the uncompressed and compressed parts of the element, respectively, $A_1(t)$ and $A_2(t)$ are the areas of the electrodes of the uncompressed and compressed parts of the element, respectively (note that $A_1 + A_2 = A$, the total electrode area), d is the ferroelectric element thickness, ϵ_1 and ϵ_2 are the relative dielectric permittivity of the uncompressed and compressed zones, respectively, and ϵ_0 is the dielectric permittivity of free space.

The system of Eqs. (3) and (4) was solved using an iterative method. At the first iteration, the permittivity of the uncompressed part of the PZT 95/5 element was taken at a low electric field, $\epsilon_1 = 305$. The permittivity of the compressed PZT 95/5 was $\epsilon_2 = 270$.^{20,21} Re-polarization of the compressed part of the element under a high electric field is not likely because the state of depolarization is stabilized by the applied stress. The first iteration results indicate that at $t = 0.7 \mu$ s, the capacitance of the compressed part of the element is $C_2(0.7 \mu\text{s}) = 7 \text{ pF}$, the capacitance of the uncompressed part is $C_1(0.8 \mu\text{s}) = 37 \text{ pF}$, and the total capacitance of the element is $C_{Iter1}(0.7 \mu\text{s}) = 44 \text{ pF}$. The voltage generated by the element is $V_{Iter1}(0.7 \mu\text{s}) = 512 \text{ kV}$, and the electric field is $E_{Iter1}(0.7 \mu\text{s}) = 21.3 \text{ kV}/\text{mm}$.

The electric field obtained in the first iteration is significantly higher than the breakdown field for PZT 95/5 ceramic elements.^{1,4,5,9,24,27} When the electric field within the ferroelectric element exceeds the breakdown field, conductive channels are formed within the element body, the electrodes become short-circuited, and the voltage and electric field across the element goes down to zero in a hundred nanoseconds.^{9,24,27} According to the

experimental results,^{5,9,24,27} the breakdown field of PZT 95/5 elements with thicknesses of 20–30 mm at shock wave transit times of 0.5–1.0 μ s is in the range of 8 kV/mm, which is lower by a factor of 2.6 than the first iteration field (21.3 kV/mm).

For the second iteration, the permittivity of the uncompressed PZT 95/5 was taken from the experimental $\epsilon_1(E)$ dependence presented in Fig. 3(c), $\epsilon_1(8 \text{ kV}/\text{mm}) = 1200$, which corresponds to the permittivity at breakdown field for bulk PZT 95/5 ceramics. The permittivity of the compressed PZT 95/5 was $\epsilon_2 = 270$ (same as at the first iteration). The second iteration results indicate that $C_2(0.7 \mu\text{s}) = 7 \text{ pF}$, $C_1(0.7 \mu\text{s}) = 148 \text{ pF}$, and the total capacitance of the element is $C_{Iter2}(0.7 \mu\text{s}) = 155 \text{ pF}$ (triple the first iteration result). The voltage generated by the element is $V_{Iter2}(0.7 \mu\text{s}) = 147 \text{ kV}$, and the electric field is $E_{Iter2}(0.7 \mu\text{s}) = 6.1 \text{ kV}/\text{mm}$ (which is lower than the breakdown field). The results obtained at the third iteration were equal to those at the second iteration because there is no significant change in the PZT 95/5 permittivity at an electric field ranging from 4 to 8 kV/mm [Fig. 3(c)]: $V_{Iter3}(0.7 \mu\text{s}) = 147 \text{ kV}$ and $E_{Iter3}(0.7 \mu\text{s}) = 6.1 \text{ kV}/\text{mm}$.

Compare the calculation results with the experiment. At the shock wave transit time of 0.7 μ s, a transversely shocked PZT 95/5 element (24 \times 16 \times 25 mm³) of the shock wave driven FEG operating in the open circuit mode⁹ produced $V_{FEG}(0.7 \mu\text{s}) = 154 \text{ kV}$ and $E(0.7 \mu\text{s}) = 6.4 \text{ kV}/\text{mm}$, which are in good agreement with the third iteration results. Therefore, the system of Eqs. (3) and (4) along with the dependence of the permittivity on the electric field [Fig. 3(c)] can be used to predict the voltage and electric field generated by shock-compressed PZT 95/5 ferroelectrics at different moments of shock wave transit. It is important to note that experimentally obtained voltage and electric field generated by a shocked PZT 95/5 element⁹ are lower by a factor of 3.3 than the outputs calculated with Eq. (3) using a low-field permittivity of poled PZT 95/5 in the uncompressed zone (the first iteration results).

The energy density generated by a transversely shocked ferroelectric element operating in the open circuit mode is

$$w(t) = \frac{C_{FEG}(t) V_{FEG}^2(t)}{2 Vol}, \quad (5)$$

where $w(t)$ is the energy density of the ferroelectric element at time t and Vol is the volume of the element. The V_{FEG} and the volume of the element can be measured experimentally, while monitoring the capacitance of the element during shock wave transit is not possible. However, the element capacitance can be determined using Eqs. (4) and (5) as

$$w(t) = \frac{\epsilon_0 E_{FEG}^2(t)}{2} \left(\frac{\epsilon_1 A_1(t)}{A_1(t) + A_2(t)} + \frac{\epsilon_2 A_2(t)}{A_1(t) + A_2(t)} \right), \quad (6)$$

where $E_{FEG}(t)$ is the electric field generated within the shocked ferroelectric element [$E_{FEG}(t) = V_{FEG}(t)/d$]. Equation (6) along with the dependence of the permittivity on the electric field (Fig. 3) can be used to determine the energy density of PZT 95/5 elements during shock wave transit.

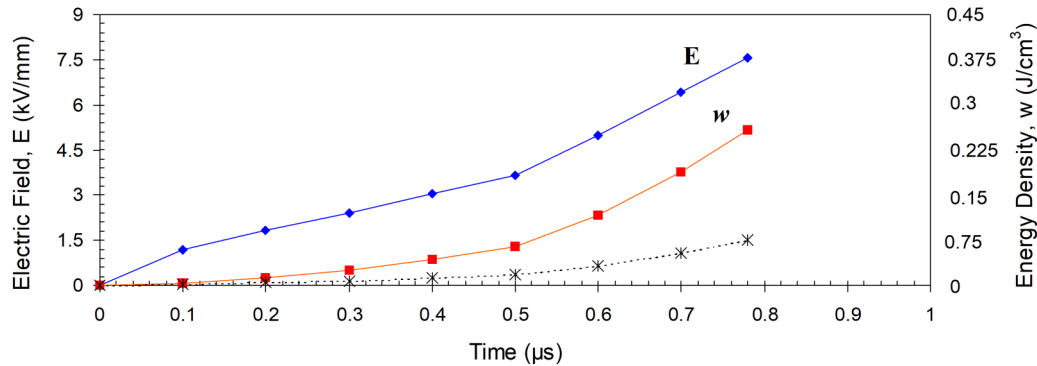


FIG. 7. Experimentally obtained electric field (diamonds) generated by a transversely shocked PZT 95/5 element ($24 \times 16 \times 25 \text{ mm}^3$) of the explosively driven FEG during shock wave transit across the element (raw data are reported in Ref. 9) and the energy density of the element (squares) determined with Eq. (6) using the dependence of the permittivity of poled uncompressed PZT 95/5 on the electric field (Fig. 3). The energy density of the element determined with Eq. (6) using a low-field permittivity of poled uncompressed PZT 95/5 ($\epsilon_1 = 305$) is shown by the asterisks.

Substituting the parameters for the experiment with the PZT 95/5 element of $24 \times 16 \times 25 \text{ mm}^3$ at the shock transit time of $0.7 \mu\text{s}$ (Ref. 9) [$E(0.7 \mu\text{s}) = 6.4 \text{ kV/mm}$, $A_1 = 3.3 \text{ cm}^2$, $A_2 = 0.7 \text{ cm}^2$] and the permittivity of the poled material in the compressed zone from the $\epsilon_1(E)$ dependence in Fig. 3 [$\epsilon_1(6.4 \text{ kV/mm}) = 1200$, $\epsilon_2 = 270$] into Eq. (6) gives a PZT 95/5 energy density of $w(0.7 \mu\text{s}) = 0.19 \text{ J/cm}^3$.

The analysis of the experimental results for the PZT 95/5 element of $24 \times 16 \times 25 \text{ mm}^3$ (Ref. 9) [$E(0.7 \mu\text{s}) = 6.4 \text{ kV/mm}$, $A_1 = 3.3 \text{ cm}^2$, $A_2 = 0.7 \text{ cm}^2$] with Eq. (6) using a low-field permittivity of the poled material in the compressed zone [$\epsilon_1 = 305$, $\epsilon_2 = 270$] gives a PZT 95/5 energy density of $w(0.7 \mu\text{s}) = 0.054 \text{ J/cm}^3$; i.e., taking into consideration the dependence of the permittivity on electric field makes a significant difference in the energy density of shocked ferroelectrics.

Note that in an ideal situation, the electric field within the ferroelectric element is not limited by the electric breakdown and the permittivity of poled ferroelectric in the uncompressed zone does not depend on the electric field. In this case, the ferroelectric element would be capable of producing $E_{\text{Iter1}}(0.7 \mu\text{s}) = 21.3 \text{ kV/mm}$. Substituting the “ideal” parameters [$E_{\text{Iter1}}(0.7 \mu\text{s}) = 21.3 \text{ kV/mm}$, $\epsilon_1 = 305$, $\epsilon_2 = 270$, $A_1 = 3.3 \text{ cm}^2$, $A_2 = 0.7 \text{ cm}^2$] into Eq. (6) gives an energy density of 0.6 J/cm^3 .

Figure 7 shows the experimentally obtained electric field generated by a transversely shocked PZT 95/5 element ($24 \times 16 \times 25 \text{ mm}^3$) of the shock wave driven FEG during shock wave transit across the element⁹ and the energy density of the element determined with Eq. (6) using the dependence of the permittivity of poled uncompressed PZT 95/5 on the electric field [Fig. 3(c)]. The energy density of the element increases from 0.09 to 0.26 J/cm^3 over the shock wave transit time. Figure 7 also shows the energy density of the element determined with Eq. (6) using a low-field permittivity of poled uncompressed PZT 95/5 ($\epsilon_1 = 305$). This energy density is lower by a factor of 3.5 than that determined with the electric-field-dependent permittivity.

V. CONCLUSIONS

The dielectric permittivity of poled ferroelectric ceramics, films, and single crystals under pulsed high electric fields was investigated experimentally. The experimental data indicate that the application of the pulsed electric field ranging from 0.1 to 10 kV/mm results in a fourfold increase in the relative permittivity of PZT 95/5 ceramics and films (from 300 to 1200) and a threefold increase in the permittivity of rhombohedral single-domain 0.27PIN-PMN-0.26PT crystals (from 720 to 2100), while an electric field does not have a significant impact on the permittivity of PZT 52/48 ceramics or multi-domain 0.27PIN-PMN-0.26PT and 0.68PMN-0.32PT crystals. The results of measurements of capacitances of PZT 95/5 ceramics and single-domain 0.27PIN-PMN-0.26PT crystals at low electric fields indicate that after the high voltage pulse, the low-field permittivity of these ferroelectrics returned to its original value. An increase in the permittivity under high electric fields might have a significant impact on the output characteristics of ferroelectric systems. The results obtained in this study can be used for the analysis of high-power and low-power ferroelectric devices operating at high electric fields.

AUTHOR DECLARATIONS

Conflict of Interest

The authors have no conflicts to disclose.

Author Contributions

Sergey I. Shkuratov: Formal analysis (equal); Investigation (equal); Methodology (lead); Project administration (lead); Writing – original draft (equal); Writing – review & editing (equal). **Jason Baird:** Formal analysis (equal); Writing – original draft (equal); Writing – review & editing (equal). **Vladimir G. Antipov:** Formal analysis (equal); Investigation (equal); Writing – original draft (equal). **Christopher S. Lynch:** Formal analysis (equal); Writing – original draft (equal); Writing – review & editing (equal).

26 March 2024 21:11:50

DATA AVAILABILITY

The data that support the findings of this study are available within the article.

REFERENCES

- ¹P. C. Lysne and C. M. Percival, "Electric energy generation by shock compression of ferroelectric ceramics: Normal-mode response of PZT 95/5," *J. Appl. Phys.* **46**(4), 1519–1525 (1975).
- ²R. E. Setchell, "Shock wave compression of the ferroelectric ceramic $\text{Pb}_{0.99}(\text{Zr}_{0.95}\text{Ti}_{0.05})_{0.98}\text{Nb}_{0.02}\text{O}_3$: Depoling currents," *J. Appl. Phys.* **97**, 013507 (2005).
- ³D. Jiang, Y. Feng, J. Du, and Y. Gu, "Shock-wave- and hydrostatic-pressure-induced depolarization of $\text{Pb}(\text{Zr},\text{Sn},\text{Ti})\text{O}_3$ for pulse power applications," *High Pressure Res.* **31**(3), 436–444 (2011).
- ⁴L. L. Altgilbers, J. Baird, B. Freeman, C. S. Lynch, and S. I. Shkuratov, *Explosive Pulsed Power* (Imperial College Press, London, 2010).
- ⁵S. I. Shkuratov, *Explosive Ferroelectric Generators: From Physical Principles to Engineering* (World Scientific Publishing Co., 2019).
- ⁶P. Peng, H. Nie, G. Wang, Z. Liu, F. Cao, and X. Dong, "Shock-driven depolarization behavior in BNT-based lead-free ceramics," *Appl. Phys. Lett.* **113**, 082901 (2018).
- ⁷Z. Gao, W. Peng, B. Chen, S. A. T. Redfern, K. Wang, B. Chu, Q. He, Y. Sun, X. Chen, H. Nie, W. Deng, L. Zhang, H. He, G. Wang, and X. Dong, "Giant power output in lead-free ferroelectrics by shock-induced phase transition," *Phys. Rev. Mat.* **3**, 035401 (2019).
- ⁸Z. Liu, T. Lu, F. Xue, H. Nie, R. Withers, A. Studer, F. Kremer, N. Narayanan, X. Dong, D. Yu, L. Chen, Y. Liu, and G. Wang, "Lead-free $(\text{Ag},\text{K})\text{NbO}_3$ materials for high-performance explosive energy conversion," *Sci. Adv.* **6**(21), eaba0367 (2020).
- ⁹S. I. Shkuratov, J. Baird, and V. G. Antipov, "Effect of shock vector/polarization vector configuration on the generation of ultrahigh voltage by adiabatically compressed ferroelectric materials," *Appl. Phys. Lett.* **119**, 092903 (2021).
- ¹⁰S. I. Shkuratov, J. Baird, V. G. Antipov, S. Zhang, and J. B. Chase, "Multilayer PZT 95/5 antiferroelectric film energy storage devices with giant power density," *Adv. Mater.* **31**, 1904819 (2019).
- ¹¹Z. Zhou, L. Fang, Z. Xiong, Y. Zhang, Y. Liu, G. Liu, Y. Liu, R. He, T. Han, J. Li, K. Wang, and Z. Gao, "Phase transition of potassium sodium niobate under high pressures," *Appl. Phys. Lett.* **123**, 012904 (2023).
- ¹²J. Gao, L. Xie, H. Zhang, J. Yu, G. Liu, G. Wang, J. Bai, Y. Gu, and H. He, "The charge release and its mechanism for $\text{Pb}(\text{In}_{1/2}\text{Nb}_{1/2})-\text{Pb}(\text{Mg}_{1/3}\text{Nb}_{2/3})-\text{PbTiO}_3$ ferroelectric crystals under one-dimensional shock wave compression," *J. Am. Ceram. Soc.* **98**(3), 855–860 (2015).
- ¹³S. I. Shkuratov, J. Baird, V. G. Antipov, and J. B. Chase, "Generation of giant electric energy density by adiabatically compressed PIN-PMN-PT ferroelectric single crystals," *Appl. Phys. Lett.* **118**, 122902 (2021).
- ¹⁴S. I. Shkuratov, J. Baird, V. G. Antipov, C. S. Lynch, S. Zhang, J. B. Chase, and H. J. Ro, "Giant power density produced by PIN-PMN-PT ferroelectric single crystals due to a pressure induced polar-to-nonpolar phase transformation," *J. Mater. Chem. A* **9**, 12307–12319 (2021).
- ¹⁵S. I. Shkuratov and C. S. Lynch, "A review of ferroelectric materials for high power devices," *J. Mater.* **8**(4), 739–752 (2022).
- ¹⁶P. C. Lysne, "Dielectric properties of shock-wave compressed PZT 95/5," *J. Appl. Phys.* **48**(3), 1020–1023 (1977).
- ¹⁷P. C. Lysne, "Shock-induced polarization of a ferroelectric ceramic," *J. Appl. Phys.* **48**(3), 1024–1031 (1977).
- ¹⁸P. C. Lysne, "Resistivity of shock-wave-compressed PZT 95/5," *J. Appl. Phys.* **48**(11), 4565–4568 (1977).
- ¹⁹R. E. Setchell, S. T. Montgomery, D. E. Cox, and M. U. Anderson, "Dielectric properties of PZT 95/5 during shock compression under high electric field," in *AIP Conference Proceedings CP845, Shock Compression of Condensed Matter—2005*, edited by M. D. Furnish, M. Elert, T. P. Russell, and C. T. White (American Institute of Physics, 2006), pp. 278–281.
- ²⁰Y. Wu, G. Liu, Z. Gao, H. He, and J. Deng, "Dynamic dielectric properties of the ferroelectric ceramic $\text{Pb}(\text{Zr}_{0.95}\text{Ti}_{0.05})\text{O}_3$ in shock compression under high electrical field," *J. Appl. Phys.* **123**, 244102 (2018).
- ²¹J. C. Valadez, R. Sahul, E. Alberta, W. Hackenberger, and C. S. Lynch, "The effect of a hydrostatic pressure induced phase transformation on the unipolar electrical response of Nb modified 95/5 lead zirconate titanate," *J. Appl. Phys.* **111**, 024109 (2012).
- ²²J. Fritz, "Uniaxial-stress effects in 95/5 lead zirconate titanate ceramic," *J. Appl. Phys.* **49**(9), 4922–4928 (1978).
- ²³H. R. Jo and C. S. Lynch, "Effect of composition on the pressure-driven ferroelectric to antiferroelectric phase transformation behavior of $(\text{Pb}_{0.97}\text{La}_{0.02})(\text{Zr}_{1-x-y}\text{Sn}_x\text{Ti}_y)\text{O}_3$ ceramics," *J. Appl. Phys.* **116**, 074107 (2014).
- ²⁴S. I. Shkuratov, J. Baird, V. G. Antipov, and J. B. Chase, "The dependence of breakdown field upon breakdown delay time in adiabatically compressed ferroelectric ceramics," *Appl. Phys. Lett.* **115**, 022903 (2019).
- ²⁵M. Si, A. Murray, Z. Lin, J. Andler, J. Li, J. Noh, S. Alajlouni, C. Niu, X. Lyu, D. Zheng, K. Maize, A. Shakouri, S. Datta, R. Agrawal, and P. D. Ye, "BEOL compatible indium-tin-oxide transistors: Switching of ultrahigh-density 2-D electron gas over $0.8 \times 10^{14}/\text{cm}^2$ at oxide/oxide interface by the change of ferroelectric polarization," *IEEE Trans. Electron Devices* **68**(7), 3195–3199 (2021).
- ²⁶H. G. Beom, K. M. Jeong, J. Y. Park, S. Lin, and G. H. Kim, "Electrical failure of piezoelectric ceramics with a conductive crack under electric fields," *Eng. Fract. Mech.* **76**(15), 2399–2407 (2009).
- ²⁷S. Lin, H. G. Beom, and D. Tao, "Tubular channel growth in piezoelectric ceramics under electric fields," *Acta Mech.* **210**, 47–55 (2010).
- ²⁸B. Jaffe, W. R. Cook, and H. Jaffe, *Piezoelectric Ceramics* (Academic Press, London, 1971).
- ²⁹P. Finkel, C. Lynch, and A. Amin, "Transduction modality near instability in domain engineered relaxor ferroelectric single crystals," *Smart Mater. Struct.* **33**(1), 013001 (2024).
- ³⁰A. J. Moulson and J. M. Herbert, *Electroceramics: Materials, Properties, Applications* (John Wiley & Sons, 2003).
- ³¹S. Thapliyal, P. Agrawal, P. Agrawal, S. S. Nene, R. S. Mishra, B. A. McWilliams, and K. C. Cho, "Segregation engineering of grain boundaries of a metastable Fe-Mn-Co-Cr-Si high entropy alloy with laser-powder bed fusion additive manufacturing," *Acta Mater.* **219**, 117271 (2021).

26 March 2024 21:11:50